PROCEEDINGS
Of SPIE-The International Society for Optical Engineering

Volume 502

Optical Materials Technology for Energy Efficiency and Solar Energy Conversion III

Carl M. Lampert
Chairman/Editor

Cooperating Organizations
American Solar Energy Society • International Solar Energy Society
U.S. Department of Energy, Office of Solar Heat Technologies
Optical Sciences Center/University of Arizona • Institute of Optics/University of Rochester

August 21-23, 1984
San Diego, California

Proceedings of SPIE—The International Society for Optical Engineering

Volume 502

Optical Materials Technology for Energy Efficiency and Solar Energy Conversion III

Carl M. Lampert
Chairman/Editor

Cooperating Organizations
American Solar Energy Society • International Solar Energy Society
U.S. Department of Energy, Office of Solar Heat Technologies
Optical Sciences Center/University of Arizona • Institute of Optics/University of Rochester

August 21–23, 1984
San Diego, California

Published by
SPIE—The International Society for Optical Engineering
P.O. Box 10, Bellingham, Washington 98227-0010 USA
Telephone 206/676-3290 (Pacific Time) • Telex 46-7053

The papers appearing in this book comprise the proceedings of the meeting mentioned on the cover and title page. They reflect the authors' opinions and are published as presented and without change, in the interests of timely dissemination. Their inclusion in this publication does not necessarily constitute endorsement by the editors or by SPIE.

Please use the following format to cite material from this book:
Author(s), "Title of Paper," *Optical Materials Technology for Energy Efficiency and Solar Energy Conversion III,* Carl M. Lampert, Editor, Proc. SPIE 502, page numbers (1984).

Library of Congress Catalog Card No. 84-72610
ISBN 0-89252-537-1

Printed in the United States of America.

OPTICAL MATERIALS TECHNOLOGY FOR ENERGY EFFICIENCY AND SOLAR ENERGY CONVERSION III

Volume 502

Conference Committee

Chairman
Carl M. Lampert
Lawrence Berkeley Laboratory

Co-Chairmen
Claes G. Granqvist
Chalmers University of Technology, Sweden

Stan W. Moore
Los Alamos National Laboratory

David M. Pellish
U.S. Department of Energy

Stephen E. Selkowitz
Lawrence Berkeley Laboratory

Volker Wittwer
Fraunhofer Institut für Solare Energiesysteme, West Germany

B. O. Seraphin
Optical Sciences Center/University of Arizona

Session Chairmen
Session 1—Transparent Heat Mirror Films
B. O. Seraphin, Optical Sciences Center/University of Arizona

Session 2—Optical Switching Materials
Claes G. Granqvist, Chalmers University of Technology, Sweden
Carl M. Lampert, Lawrence Berkeley Laboratory

Session 3—Selective Absorber Coatings
Stan W. Moore, Los Alamos National Laboratory

Session 4—General Solar Optical Materials and Instrumentation
Volker Wittwer, Fraunhofer Institut für Solare Energiesysteme, West Germany

International Forum—Technical Needs of the Energy Related Coatings Industry and the Building Sciences
Stephen E. Selkowitz, Lawrence Berkeley Laboratory
Carl M. Lampert, Lawrence Berkeley Laboratory
David M. Pellish, U.S. Department of Energy

OPTICAL MATERIALS TECHNOLOGY FOR ENERGY EFFICIENCY AND SOLAR ENERGY CONVERSION III

Volume 502

INTRODUCTION

Large-scale optical materials play a vital role in the performance of energy conserving architectural windows, and offer increased efficiency to solar energy conversion systems. New materials and improved existing materials can allow for totally new designs or upgrade current solar conversion and glazing systems. Increases in efficiency, stability and durability are key areas for solar optical materials research. In general, these materials perform in a much more aggressive environment than conventional optics do. The scope of this conference was to cover the recent advances in optical materials including heat mirrors, switching coatings, solar absorbers, generalized solar materials, and instrumentation.

Transparent heat mirrors are used to selectively reflect infrared energy while maintaining high visible transparency. The importance of band-gap widening in heavily doped semiconductors used as heat mirrors was covered in Session 1. Also large-scale production issues pertaining to multilayer heat mirrors were given; a few years ago, large-scale production of these coatings was unheard of. A related and very popular Session 2 was on optical switching films. Within this exciting session, electrochromism of tungsten oxide was discussed for the control of visible and near-infrared energy passing through a glazing. There remains a wide range of materials which science research needs to aid in the understanding of the electrochromic phenomena, its device operation and limitations.

Solar absorbers are still a popular research technology. They are the most advanced and diverse of the solar optical selective materials. In Session 3 on absorbers, progress on wavelength selective paints was presented. After many years of research, progress in this area has been quite successful, with coatings that rival conventional electroplated deposits. Other key interest areas are multilayer interference absorber coatings, absorbers using fluidized particles, and new absorbers absorption using fluidized particle, and new absorbers based on titanium oxynitrides. Optical absorbers that can withstand high temperatures, fluxes and environmental impacts are important materials for further research.

Session 4 on generalized optical materials includes a wide range of popular subjects dealing with different solar conversion technologies. Examples are fluorinated polymer glazings, transparent aerogel insulation, amorphous silicon, evacuated glazings, and chalcogenide glass photoelectrodes. Large scale testing of solar materials is an active and challenging field. Various techniques were also covered in this session.

A special International Forum was conducted to go beyond the technical sessions and provided the participants with information on broad-based solar research in various countries and commercial experiences relating to materials needs; a few of those presentations are shown here.

This proceedings serves as a timely companion to the SPIE proceedings, Vol. 324 of January 1982, and Vol. 428 of August 1983, both dealing with optical materials technology for glazings and solar energy conversion.

Carl M. Lampert
Lawrence Berkeley Laboratory

OPTICAL MATERIALS TECHNOLOGY FOR ENERGY EFFICIENCY AND SOLAR ENERGY CONVERSION III

Volume 502

Contents

OPTICAL MATERIALS TECHNOLOGY FOR ENERGY EFFICIENCY AND SOLAR ENERGY CONVERSION III

Volume 502

Session 1

Transparent Heat Mirror Films

Chairman
B. O. Seraphin
Optical Sciences Center/University of Arizona

Bandgap widening in heavily doped oxide semiconductors used as transparent heat-reflectors

I. Hamberg and C.G. Granqvist

Physics Department, Chalmers University of Technology, S-412 96 Gothenburg, Sweden

K.-F. Berggren, B.E. Sernelius and L. Engström

Theoretical Physics Group, Department of Physics and Measurement Technology
Linköping University, S-581 83 Linköping, Sweden

Abstract

Doped oxide semiconductors, which are widely used as transparent heat-reflectors, have a wider energy gap than the undoped material. This bandgap widening was investigated in In_2O_3 and In_2O_3:Sn. Empirical data were extracted for coatings with electron density $\lesssim 10^{21}$ cm^{-3}. They are interpreted within an effective-mass-model for n-doped semiconductors well above the Mott critical density. The impurities are ionized and the associated electrons occupy the bottom of the conduction band in the form of an electron gas. The model accounts for a Burstein-Moss shift as well as electron-electron and electron-impurity scattering treated in the Random Phase Approximation. Experiments and theory were reconciled by assuming a parabolic valence band with an effective mass ~ 0.6 m. Earlier work on doped oxide semiconductors are assessed and criticized in the light of the present results.

1. Introduction and summary

In this paper we analyze bandgap widening, which is an important effect in doped oxide semiconductors used as transparent heat-reflectors. New optical data, analysis techniques, and a detailed theoretical model are discussed, and inconsistencies in earlier work are pointed out.

Transparent heat-reflectors are needed for creating energy-efficient windows with low thermal emittance, as well as for numerous other applications related to energy efficiency.[1-7] The materials with highest performance in terms of short-wavelength transmittance and long-wavelength reflectance are heavily doped oxide semiconductors based on Zn, Cd, In, Sn, and compounds of these. These oxides exhibit a very favourable combination of properties, which is the reason for their usefulness:

(i) the undoped materials have a direct bandgap $\gtrsim 3$ eV thus allowing transmission of solar and luminous radiation;
(ii) doping can be achieved to a sufficient level that the needed infrared reflectance is reached;
(iii) doping does not lead to adverse effects with regard to short-wavelength transmission, i.e., defect states within the bandgap are insignificant, and the bandgap does not get narrower; and
(iv) durability is sufficient for many important applications.

Below we focus on one specific - though prevalent - phenomenon namely the widening of the bandgap which accompanies the doping and guarantees that the oxides remain transparent. The bandgap widening by no means is a new effect, but it has been observed and investigated in earlier work on ZnO (Refs. 8,9), CdO (Ref. 10), In_2O_3 (Refs. 4, 11-21), SnO_2 (Refs. 14, 22-27), and Cd_2SnO_4 (Refs. 28-30). Much of this work is amenable to criticism on several grounds. In particular we note that (with one exception[10]) the actual magnitude of the optical bandgap has been evaluated by coarse and inadequate procedures, and that the interpretation of the bandgap (again with one exception[8]) has been made solely with regard to the Burstein-Moss effect,[31] which is often an unwarranted simplification. The purpose of this paper is to present an improved analysis of the bandgap, and to use this for interpreting the bandgap shift in high-quality films of In_2O_3:Sn (also known as Indium-Tin-Oxide or ITO). This work may be viewed as a continuation and extension of earlier studies of ours[32-36] on In_2O_3:Sn films.

In Sec. 2 below we review some earlier data on bandgap widening in doped oxide semiconductors with particular regard to our own results[36] on In_2O_3:Sn. It will be seen that the shift can be as large as ~ 0.8 eV for carrier densities of $\sim 10^{21}$ cm^{-3} in the latter material. With the aim of giving a basic explanation of this phenomenon we outline in Sec. 3 a theory[37] which includes the Burstein-Moss effect and self-energies due to electron-electron and electron-impurity scattering. The calculations are based on an effective-mass-model for n-doped semiconductors well above the Mott critical density[38,39] and are performed within the framework of the Random Phase Approximation.[40] A comparison

of experimental and theoretical results on the bandgap widening is presented in Sec. 4. We first outline a theoretical model - based on time-dependent perturbation theory - to extract a unique optical bandgap. These data are then found to be in excellent agreement with computations provided that the valence band of In_2O_3:Sn is taken to be parabolic with an effective mass ~ 0.6 m (where m is the free-electron mass).

The present analysis provides a consistent model for the optical properties of In_2O_3:Sn around its fundamental bandgap. It embraces doping of a host semiconductor to achieve a high density of electrons and accounts for their scattering against the ensuing ionized impurities. This is precisely the conceptual model used by us to explain the optical performance in the infrared.[35] Our work is confined to In_2O_3:Sn, but we are confident that the same general notions are applicable to other heavily doped oxide semiconductors. We are thus establishing a model capable of explaining the key properties of transparent heat-reflectors and transparent conductors of the doped-semiconductor-type: a high transmittance between a properly shifted and broadened energy gap and the plasma wavelength, and a high reflectance and concomitant high conductivity beyond the plasma wavelength.

2. Data on bandgap widening

There is a large body of information on bandgap widening in doped oxide semiconductors used as transparent heat-reflectors.[4,8-30] Much of this work is not very useful for a detailed analysis, though, since in most cases the bandgap shift is inferred either from directly observed changes in transmittance spectra or from plots of absorption coefficient (α) against photon energy ($\hbar\omega$) within undesirably narrow energy ranges. In particular, there are numerous cases in which the bandgap is taken to be the extrapolated zero-energy intercept in plots of α^2 versus $\hbar\omega$. Apparently, it has seldom been realized that for heavily doped crystalline semiconductors this procedure does not yield the direct optical bandgap, if this quantity is defined in the usual manner as the minimum energy for quantum-mechanically allowed transitions between a filled valence band and empty states in a conduction band.

Notwithstanding the somewhat discouraging experimental situation, there are a few earlier investigations which yield detailed insight into the bandgap widening. Especially we wish to draw attention to some rather old work by Finkenrath[10] on non-stoichiometric CdO films prepared by sputtering. Figure 1, which is based on this work, shows that the onset of strong absorption moves monotonically towards higher energy as the electron density (n_e) goes up. The shift is exceptionally strong for CdO (Ref. 10) and Cd_2SnO_4 (Refs. 28-30). We note that the bandgap widening is essential for producing films which are not strongly absorbing for solar radiation. Figure 2, redrawn from a recent work by Shanti et al.,[25] pertains to SnO_2:Sb. We observe again that the onset of absorption goes towards higher energy in the more strongly doped specimens.

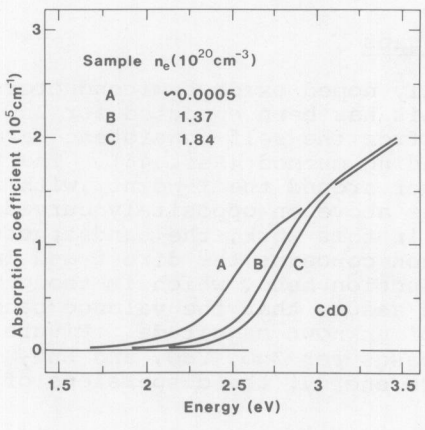

Figure 1. Spectral absorption coefficient for non-stoichiometric CdO films with different electron densities (replotted from Ref. 10).

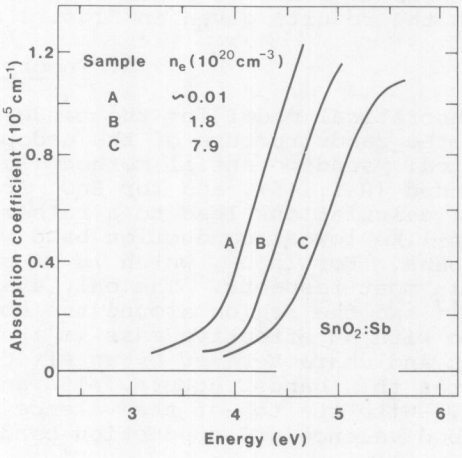

Figure 2. Spectral absorption coefficient for Sb-doped SnO_2 films with different electron densities (replotted from Ref. 25).

Rather than trying to understand the available data on bandgap widening, we investigated new samples of high-quality In_2O_3:Sn. These were made by reactive electron-beam deposition of pure In_2O_3 and of In_2O_3 with up to 9 mol. % SnO_2 onto substrates of CaF_2. The deposition conditions (evaporation rate, reactive gas pressure, substrate temperature, etc) required for optimum performance are detailed elsewhere.[32] Spectral normal transmittance and near-normal reflectance were recorded by spectrophotometry. Figure 3 shows data for a

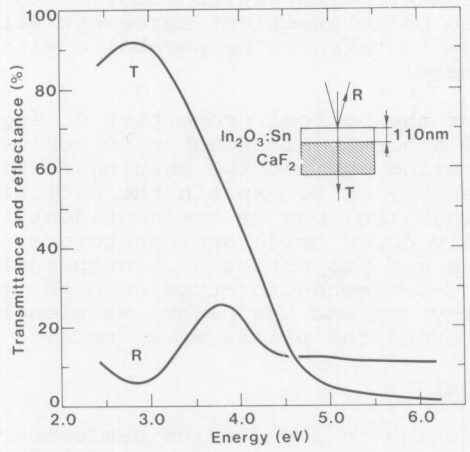

Figure 3. Spectral transmittance (T) and reflectance (R) for a film of In_2O_3:Sn. The measurement configuration is sketched in the inset.

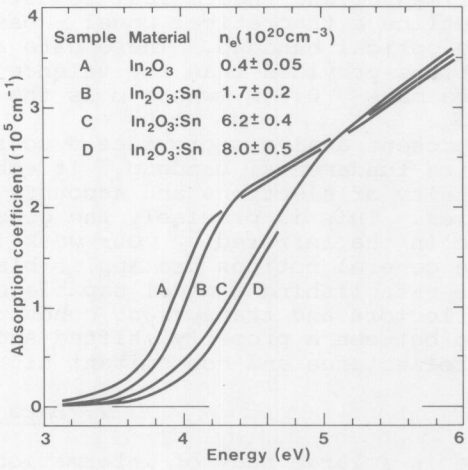

Figure 4. Spectral absorption coefficient for films of In_2O_3 and In_2O_3:Sn. Inset table shows the electron densities in the various films.

110-nm-thick film of In_2O_3:Sn. The large decrease in transmittance signifies the bandgap. Oscillations in reflectance indicate optical interference.

The spectrophotometric measurements were used to extract the complex refractive indices of the various films with known techniques.[41,42] These data were then employed to calculate spectral absorption coefficients. Main part of Fig. 4 shows results for four different films prepared with In_2O_3 (curve A) and In_2O_3 + SnO_2 (curves B-D) as starting material. Similar curves have been reported by Ohhata et al.[15] It is seen that the bandgaps lie at different energies, and that the onset of strong absorption is gradual. Electron densities were obtained from determinations of the plasma energy (i.e., the energy for which the real part of the dielectric function equals zero) as described in earlier papers.[34,35] For films of pure In_2O_3 we obtain a non-zero electron density as a result of doubly charged oxygen vacancies,[43] while for Sn-doped In_2O_3 the electron density is mainly caused by Sn-atoms entering substitutionally as Sn^{4+} on In^{3+}-sites.[43] Actual magnitudes of n_e are given in the inset of Fig. 4. It is concluded that an increasing electron density leads to a progressive widening of the energy gap - which is clearly in line with the results given in Figs. 1 and 2.

3. Theory of shifted bandgaps

Our theoretical model for the bandgap shift in heavily doped oxide semiconductors is built on the bandstructure of the undoped material. This has been computed for ZnO from an empirical pseudopotential method (Ref. 44), for CdO from the self-consistent Hartree--Fock method (Ref. 45), and for SnO_2 from the tight-binding method (Ref. 46). The three different calculations lead to a rather similar behaviour around the Γ-point, with a free--electron-like lowest conduction band whose minimum lies above an oppositely curved shallower valence band. For In_2O_3, which is of primary interest in this work, the bandstructure is unknown in most respects. The only available information concerns the direct and indirect bandgaps[47] and the region around the bottom of the conduction band, which is thought to be parabolic with an effective mass (m_c^*) of[19] ~ 0.3 m. We assume that the valence band is parabolic and characterized by an effective mass (m_v^*) of unknown magnitude. Figure 5a illustrates this bandstructure. Its analogy with the cases for ZnO, CdO, and SnO_2 is apparent. With the top of the valence band as reference energy, the dispersions of the unperturbed valence and conduction bands are

$$E_v^{\,o}(k) = -\hbar^2k^2/2m_v^* \qquad (1)$$

and

$$E_c^{\,o}(k) = E_{g0} + \hbar^2k^2/2m_c^*, \qquad (1')$$

respectively. E_{g0} is the bandgap of the undoped semiconductor, k is the wavenumber, and superscript o denotes unperturbed bands. Single crystalline plates of In_2O_3 have[47] $E_{g0} = 3.75$ eV.

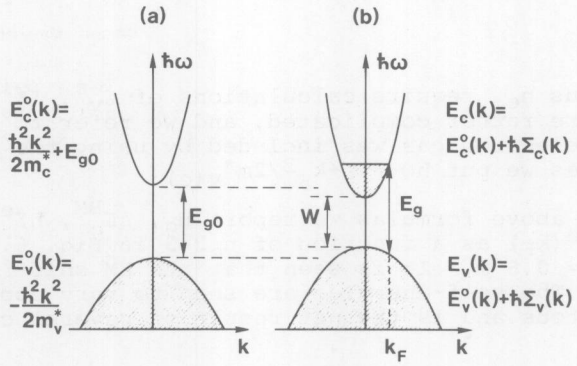

Figure 5. Assumed bandstructure of (a) In_2O_3 and (b) Sn-doped In_2O_3. Shaded areas indicate occupied states. Bandgaps, Fermi wavenumber, and dispersion relations are shown.

We now consider In_2O_3 doped to an extent that the Mott critical density[38,39] is exceeded. We then have

$$n_e >> (0.25\, m_c^* e^2/\varepsilon_o \hbar^2)^3, \tag{2}$$

where e is the electron charge, ε_o is the permettivity of free space, and $\hbar$ is Planck's constant divided by 2π. Under this condition, which is fulfilled for all of the present samples, the conduction band is partly filled - i.e., its lowest states are blocked - which leads to a widening of the optical bandgap according to the Burstein-Moss (BM) effect.[31] This widening is partially compensated by a downwards shift of the conduction band and an upwards shift of the valence band which occur as a consequence of electron-electron and electron-impurity scattering.[37,48,49] The bandgap narrowing is indicated in Fig. 5(b); it is a well known effect[50] in heavily doped Si, which has been studied recently for microelectronic device applications. We find it surprising that mechanisms for bandgap narrowing have not been invoked in earlier analyses of bandgap shifts in doped oxide semiconductors (with the exception of a study[8] of ZnO). Still another effect of the doping is that m_c^* (and perhaps also m_v^*) are dependent[19] on n_e.

Quantitative evaluations of shifted bandgaps require that we replace the bare band potentials in Eqs. (1) and (1') by the corresponding quasiparticle dispersions

$$E_v(k,\omega) = E_v^o(k) + \hbar\Sigma_v(k,\omega) \tag{3}$$

and

$$E_c(k,\omega) = E_c^o(k) + \hbar\Sigma_c(k,\omega), \tag{3'}$$

where $\hbar\Sigma_v$ and $\hbar\Sigma_c$ are self-energies due to electron-electron and electron-impurity scattering. The ensuing bandgap shift can be written

$$E_g = E_{g0} + \Delta E_g^{BM} + \hbar\Sigma_c(k_F,\omega) - \hbar\Sigma_v(k_F,\omega), \tag{4}$$

where the BM shift is given by

$$\Delta E_g^{BM} = \frac{\hbar^2}{2}\left(\frac{1}{m_v^*} + \frac{1}{m_c^*}\right)(3\pi^2 n_e)^{2/3}, \tag{5}$$

and

$$k_F = (3\pi^2 n_e)^{1/3} \tag{6}$$

is the Fermi wavenumber. Electron-electron (ee) and electron-impurity (ei) scattering are taken as additive processes, i.e.,

$$\hbar\Sigma = \hbar\Sigma^{ee} + \hbar\Sigma^{ei}. \tag{7}$$

Explicit results of E_g versus n_e require calculations of Σ_v^{ee}, Σ_v^{ei}, Σ_c^{ee}, and Σ_c^{ei}. The procedures for doing this are rather complicated, and we refer to Refs. 36 and 37 for details. Screening in the electron gas was included by using the Random Phase Approximation.[40] In the self-energies we put $\hbar\omega = \hbar^2 k_F^2/2m^*_{v(c)}$.

As an application of the above formulas we report E_g, ΔE_g^{BM}, $\hbar\Sigma^{ei}(k_F) \equiv \hbar\Sigma_c^{ei}(k_F) - \hbar\Sigma_v^{ei}(k_F)$, and $\hbar\Sigma^{ee}(k_F) \equiv \hbar\Sigma_c^{ee}(k_F) - \hbar\Sigma_v^{ee}(k_F)$ as a function of $n_e^{2/3}$ in Fig. 6. We used empirical data[15,19] for m_c^*, and $m_v^* = 0.6$ m. It is seen that the BM shift dominates except for the lowest electron densities. The self-energies are seen to vary approximately as $n_e^{2/3}$; this dependence is rather fortuitous and is the net result of several competing mechanisms.

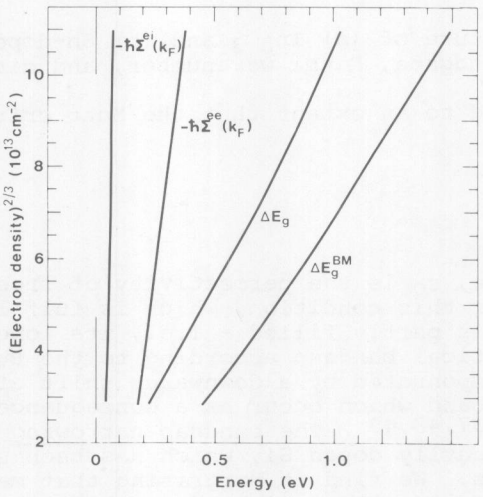

Figure 6. Computed data on optical bandgap versus electron density to the power 2/3. The contributions from the Burstein-Moss shift (ΔE_g^{BM}), electron-impurity scattering ($\hbar\Sigma^{ei}$) and electron-electron scattering ($\hbar\Sigma^{ee}$) are shown.

4. Comparison of theory and experiments for In_2O_3:Sn

The experimental data on spectral absorption coefficient - shown in Figs. 1, 2 and 4 - indicate a gradual onset of strong absorption, and it is not obvious how to locate a unique optical bandgap to be compared with E_g as derived in the preceding section. Using time--dependent perturbation theory it is straight-forward to prove[36] that

$$\alpha \propto \int_0^\infty dx (x + \hbar\omega - W)^{\frac{1}{2}} \frac{\Gamma}{x^2 + \Gamma^2} (1 - P_c), \tag{8}$$

where we have introduced the notation

$$x \equiv \frac{\hbar^2 k^2}{2}\left(\frac{1}{m_v^*} + \frac{1}{m_c^*}\right) + W - \hbar\omega, \tag{9}$$

$$x_o \equiv \Delta E_g^{BM} + W - \hbar\omega, \tag{10}$$

$$\Gamma \equiv \hbar/\tau. \tag{11}$$

Here τ represents the broadening of the initial and final states for the optical transitions, and W is the minimum distance between the valence and conduction bands (cf. Fig. 5b). The latter quantity is given by the approximate relation

$$W \approx E_{g0} + \hbar\Sigma_c(k_F) - \hbar\Sigma_v(k_F). \tag{12}$$

Thermal excitations above the Fermi energy are represented by a Fermi function according to

$$P_c = \left\{ \exp\left[\left(\frac{\hbar^2 k^2}{2m_c^*} - \mu \right) / k_B T \right] + 1 \right\}^{-1}, \tag{13}$$

where $k_B T$ is Boltzmann's constant times the temperature and μ is the chemical potential. At $k_B T << \hbar^2 k_F^2 / 2m_c^* \equiv \varepsilon_F$ we have

$$\mu \approx \varepsilon_F \left[1 - \frac{\pi^2}{3} \left(\frac{k_B T}{2\varepsilon_F} \right)^2 \right]. \tag{14}$$

Equations (8) - (14) give a complete scheme for computing the spectral absorption coefficient in terms of two parameters. One of these is taken as $W + \Delta E_g^{BM}$. It gives the energy around which the transition from low to high absorption is centered. This parameter is convenient since it can be directly compared with E_g as computed in the preceding section. The second parameter is Γ, which gives the width of the transition.

Figure 7 shows comparisons between theory and experiments for two of the samples, whose spectral absorption coefficients were earlier given in Fig. 4. Open and filled circles correspond to evaluations based on spectrophotometric measurements. Solid curves denote theoretical data, which have been fitted by selecting appropriate magnitudes of $W + \Delta E_g^{BM}$ and Γ. In doing this fitting we have primarily regarded the middle parts of the curves. It is seen from Fig. 7 that theory and experiments can be brought in good agreement around the steepest parts of the curves, whereas the "tails" towards high and low energy cannot be reproduced to an equal precision. One of the possible reasons for this is that we have ignored the k-dependence of Γ and $\hbar\Sigma$. The dashed curves pertain to alternative values of Γ. It is apparent that the computed curves are strongly dependent on Γ and, conversely, that reasonably unique Γ's can be extracted from the experiments. When including a finite temperature we have used T = 300 K. This parameter has a marginal influence on the curve shapes, since the degeneracy temperature of the electron gas is much higher than 300 K. Table I contains $W + \Delta E_g^{BM}$ and Γ as obtained from "best fits" between theory and experiments. It is inferred that the magnitude of both parameters goes up with increasing electron density.

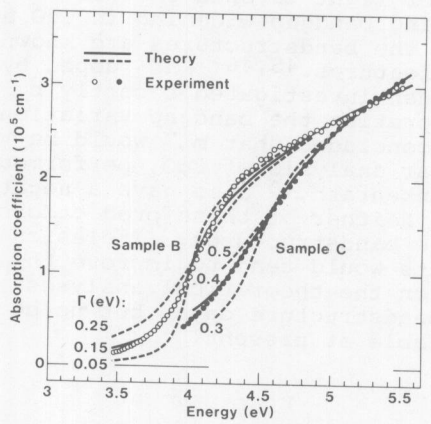

Figure 7. Spectral absorption coefficient for films of In_2O_3:Sn. Circles refer to experimental data. Solid and dashed curves were computed by using $W + \Delta E_g^{BM}$ = 4.04 eV and 4.46 eV, together with the shown magnitudes of Γ.

Table 1. Parameters used for fitting theoretical curves to experimental spectral absorption coefficients.

Sample	$W + \Delta E_g^{BM}$ [eV]	Γ [eV]
A	3.88	0.07
B	4.04	0.13
C	4.46	0.37
D	∿ 4.55	∿ 0.35

In figure 8 we compare the evaluations of $W + \Delta E_g^{BM}$ with computations of E_g. From attempts to produce good fits it became clear that m_v^* should be chosen in the range ∿0.6 - 0.7 m. For m_v^* = 0.7 we obtain best agreement by setting E_{g0} = 3.82 eV. For m_v^* = 0.6 m the corresponding energy is 3.75 eV. Thus it appears that we have to assume a bandgap for the undoped material which is either the same or somewhat higher than the value 3.75 eV pertaining to[47] single crystalline In_2O_3. The parameter Γ is governed to a large extent by ionized impurity scattering, although additional scattering mechanisms seem to be present particularly at high electron densities. Arguments behind these assessments are given in

Ref. 36.

As a final point we note from Fig. 8 that the optical bandgap scales approximately with $n_e^{2/3}$. This relation is to be expected from the BM shift (cf. Eq. 5), which has led to the erroneous conclusion - iterated in numerous papers[4,11-21] - that the BM shift alone would determine the bandgap widening. If, for the sake of argument, we neglect the self-energy effects, we can get agreement between theory and experiments only by assuming a negative magnitude of m_v^* somewhere between $\sim$-0.6 and $\sim$-1.0 m. This would imply that the valence band is curved in the same direction as the conduction band. Inclusion of the self-energies leads to a positive value of m_v^*, as discussed above. This proves the importance of considering electron-electron and electron--impurity scattering, and that qualitative differences can occur if they are neglected. Further light is shed on this issue by considering bandgap widening in CdO and SnO_2, for which the bandstructures are known in their main features.[45,46] SnO_2 doped by F and Sb has been investigated recently by Shanti et al.[25] Interpreting the bandgap variation as a BM shift, they concluded that m_v^* would be $\sim$-0.9 m. A similar analysis of CdO, performed much earlier by Finkenrath,[10] also gave a negative value of m_v^*. Neither of these predictions are corroborated by the bandstructures. Inclusion of self-energy effects would tend to improve the correspondence between the theoretical analyses of shifted bandgaps and bandstructure data, but no detailed results are available at present

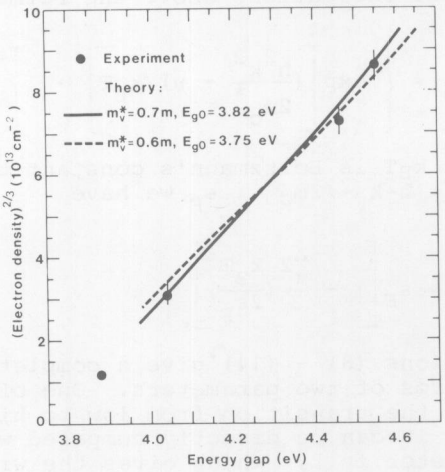

Figure 8. Electron density to the power 2/3 versus energy gap for films of In_2O_3 and In_2O_3:Sn. Circles represent experimental data (cf. Table 1). Vertical bars denote the uncertainty in extracting n_e from observed plasma energy. Solid and dashed curves indicate the results of computations using the shown values of m_v^* and E_{g0}.

Acknowledgment

This work was financially supported by grants from the Swedish Natural Science Research Council and the National Swedish Board for Technical Development.

References

1. C.G. Granqvist, Appl. Opt. 20, 2606 (1981).
2. C.M. Lampert, Solar Energy Mater. 6, 1 (1981).
3. H. Köstlin, Festkörperprobleme 22, 229 (1982).
4. K.L. Chopra, S. Major and D.K. Pandya, Thin Solid Films 102, 1 (1983).
5. C.M. Lampert, Energy Research 7, 359 (1983).
6. C.G. Granqvist, Proc. SPIE 401, 330 (1983).
7. C.G. Granqvist, The Physics Teacher, to be published.
8. A.P. Roth, J.B. Webbs, and D.F. Williams, Solid State Commun. 39, 1269 (1981); Phys. Rev. B25, 7836 (1982).
9. O. Carporaletti, Solar Energy Mater. 7, 65 (1982).
10. H. Finkenrath, Z. Phys. 159, 112 (1960).
11. V.M. Vainshtein and V.I. Fistul', Fiz. Tekh. Polup. 1, 135 (1967) [Soviet Phys. Semicond. 1, 104 (1967)].
12. H. Köstlin, R. Jost and W. Lems, Phys. Stat. Sol. A29, 87 (1975).
13. W.G. Haines and R.H. Bube, J. Appl. Phys. 49, 304 (1978).
14. J.-C. Manifacier, L. Szepessy, J.F. Bresse, M. Perotin and R. Stuck, Mater. Res. Bull. 14, 163 (1979).
15. Y. Ohhata, F. Shinoki and S. Yoshida, Thin Solid Films 59, 255 (1979).
16. A.J. Steckl and G. Mohammed, J. Appl. Phys. 51, 3890 (1980).
17. M. Mizuhashi, Thin Solid Films 70, 91 (1980).
18. F.T.J. Smith and S.L. Lyu, J. Electrochem. Soc. 128, 2388 (1981).
19. Z.M. Jarzebski, Phys. Stat. Sol. A71, 13 (1982).
20. J. Szczyrbowski, A. Dietrich and H. Hoffman, Phys. Stat. Sol. A69, 217 (1982); A78, 243 (1983).
21. S. Ray, R. Banerjee, N. Basu, A.K. Batabyal and A.K. Barua, J. Appl. Phys. 54, 3497 (1983).
22. T. Arai, J. Phys. Soc. Japan 15, 916 (1960).
23. H. Koch, Phys. Stat. Sol. 7, 263 (1964).
24. S.P. Lyashenko and V.K. Miloslavskii, Opt. Spektrosk. 19, 108 (1965) [Opt. Spectrosc. 19, 55 (1965)].

25. E. Shanti, A. Banerjee, V. Dutta and K.L. Chopra, J. Appl. Phys. 51, 6243 (1980); 53, 1615 (1982); E. Shanti, A. Banerjee and K.L. Chopra, Thin Solid Films 88, 93 (1982).
26. K.B. Sundaram and G.K. Bhagavat, J. Phys. D 14, 921 (1981).
27. K. Suzuku and M. Mizuhashi, Thin Solid Films 97, 119 (1982).
28. A.J. Nozik, Phys. Rev. B6, 453 (1972).
29. N. Miyata, K. Miyake, K. Koga and T. Fukushima, J. Electrochem. Soc. 127, 918 (1980).
30. E. Leja, K. Budzyńska, T. Pisarkiewicz and T. Stapiński, Thin Solid Films 100, 203 (1983).
31. E. Burstein, Phys. Rev. 93, 632 (1954); T.S. Moss, Proc. Phys. Soc. London B67, 775 (1954).
32. I. Hamberg, A. Hjortsberg and C.G. Granqvist, Appl. Phys. Lett. 40, 362 (1982); Proc. SPIE 324, 31 (1982).
33. I. Hamberg and C.G. Granqvist, Appl. Opt. 22, 609 (1983).
34. I. Hamberg and C.G. Granqvist, Thin Solid Films 105, L83 (1983).
35. I. Hamberg and C.G. Granqvist, Proc. SPIE 428, 2 (1983); Appl. Phys. Lett. 44, 721 (1984); Solar Energy Mater., to be published.
36. I. Hamberg, C.G. Granqvist, K.-F. Berggren, B.E. Sernelius and L. Engström, Phys. Rev. B, to be published.
37. K.-F. Berggren and B.E. Sernelius, Phys. Rev. B24, 1971 (1981).
38. N.F. Mott, Metal-Insulator Transitions (Taylor and Francis, London, 1974).
39. P.P. Edwards and M.J. Sienko, Phys. Rev. B17, 2575 (1978).
40. See, for example, G.D. Mahan, Many-Particle Physics (Plenum, New York, 1981).
41. A. Hjortsberg, Appl. Opt. 20, 1254 (1981).
42. T.S. Eriksson and A. Hjortsberg, Proc. SPIE 428, 135 (1983).
43. G. Frank and H. Köstlin, Appl. Phys. A27, 197 (1982).
44. S. Bloom and I. Ortenburger, Phys. Stat. Sol. B58, 561 (1973).
45. J.C. Boettger and A.B. Kunz, Phys. Rev. B27, 1359 (1983).
46. J. Robertson, J. Phys. C12, 4767 (1979).
47. R.L. Weiher and R.P. Ley, J. Appl. Phys. 37, 299 (1966).
48. R.A. Abram, G.J. Rees and B.L.H. Wilson, Adv. Phys. 27, 799 (1978).
49. G.D. Mahan, J. Appl. Phys. 51, 2634 (1980).
50. L. Viña, C. Umbach, M. Cardona, A. Compaan and A. Axman, Solid State Commun. 48, 457 (1983), and references therein.

Characterization of a low emissivity coating in large scale production

Steven J. Nadel
Thomas S. Mosakowski

Technology Department, Temescal, Airco Solar Products
4020 Pike Lane, Concord, California 94520

Abstract

Optimal properties of a low emissivity coating are quantified in terms of optical, thermal and aesthetic parameters. Large scale production of a Zinc Oxide/Silver/Zinc Oxide coating deposited on glass by reactive D.C. magnetron sputtering was sampled over a six-month period. The distributions of performance parameters describing the visible and solar transmission and reflection, emissivity and film color were analyzed and related to production process variations.

Introduction

Reducing window heat loss has become a major energy conservation goal, particularly for residential applications. High performance low emissivity coatings combine maximized visible and solar transmission coupled with high long wavelength infrared reflection to provide a solution to these needs.

Coating performance is based on the fact that virtually all incident solar energy is contained in the spectral range below 2.2 microns. However, a body in thermal equilibrium at room temperature radiates thermal energy in the region between 5 and 25 microns (see figure 1).[1] According to the equations for black body radiation, the peak radiation will be between 9 and 11 microns for a temperature between 0 and 40 degrees C. Therefore, a film with high transmission below 2 microns and high infrared reflection above 5 microns will be the most energy efficient coating.

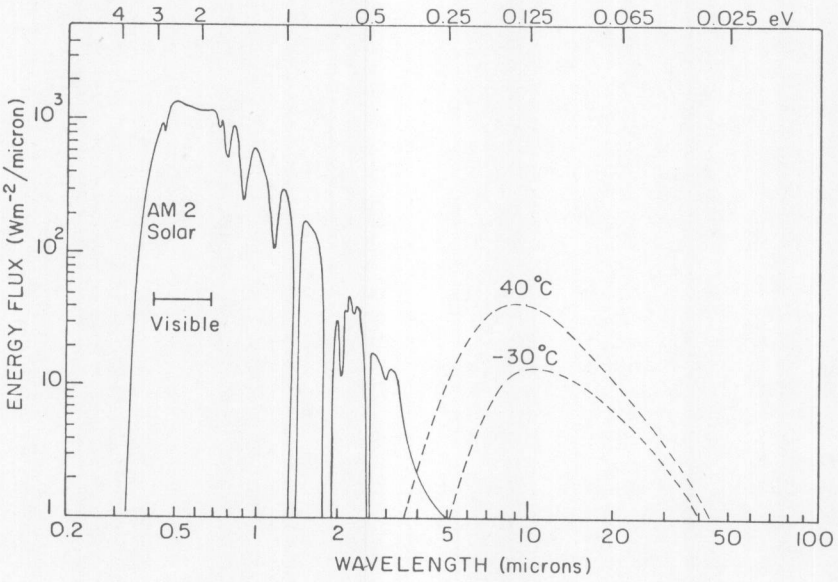

Figure 1. Solar spectrum at air mass 2 with two blackbody thermal spectra at 40 °C and -30 °C.

The production of low-e coatings

For many years, a large variety of prototypes for such coatings have been produced in laboratory scale equipment by a variety of processes, including diode, triode and magnetron sputtering, chemical spray deposition and evaporation. Prototypical systems have been either of the doped semiconductor variety (such as Indium-Tin Oxide) or of the dielectric/

metal/dielectric stack. Metals such as Cu, Ag, or Au provide the necessary infrared reflectance. However, when deposited at thicknesses needed to provide the necessary emissivity, the visible and solar transmission of these metals is too low. Enhanced transmission is provided by high index of refraction oxides such as ITO, SnO_2, Bi_2O_3, TiO_2,TaO_2, or ZnO_2 which provide dereflection in the visible/solar region. The coatings have been designed either to be directly deposited on glass or on various flexible substrates, such as mylar.

Currently, coatings of the dielectric/metal/dielectric formulation are being directly deposited on glass in high volume magnetron sputter deposition systems. The Temescal Solar Products research facility coater pictured in figure 2. contains four sputter deposition chambers, each containing two magnetron cathodes. The system is designed to allow adjacent chambers to sputter in various atmospheres, permitting metals and oxides to be deposited on line in a single pass.

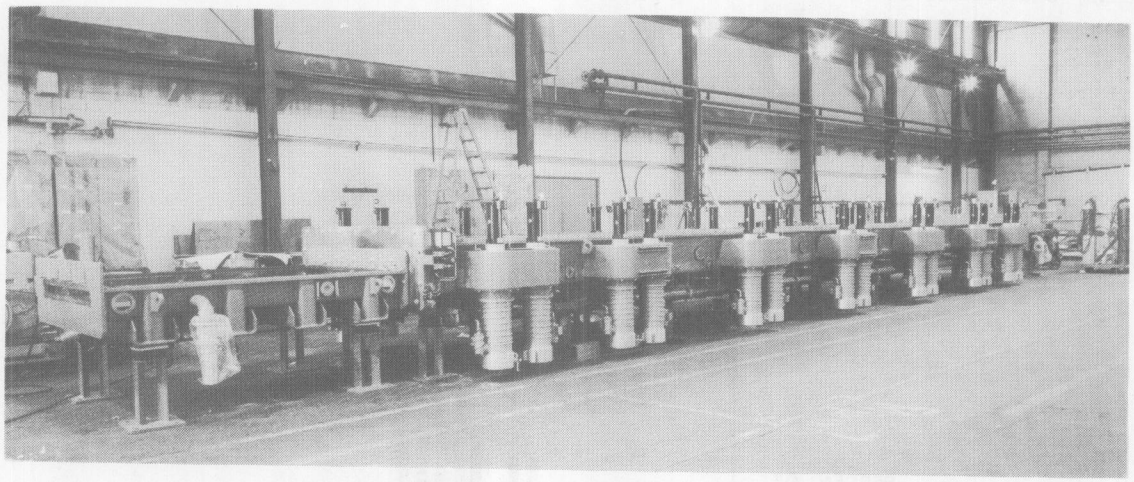

Figure 2: Temescal Research Facility Coater

For the past two years, this system has been utilized for scale up experimentation and pilot production for a $ZnO_2/Ag/ZnO_2$ low emissivity coating. For a six-month period, a large scale random sampling of this production was gathered in order to analyze the distribution and variation of performance parameters of low-emissivity coated glass. Samples were taken four times daily, eventually resulting in a set of over 250 samples. Vacuum system and sputtering process variables were carefully monitored in order to correlate production process variations to coating performance.

The performance of a low-emissivity coating is characterized by its visible transmission, film and glass side reflection, the corresponding solar properties and its emissivity.[2] For architectural and aesthetic purposes, reflected color is also a significant parameter. An ideal coating (as measured on 1/8" clear float glass) would yield visible properties of neutral reflected color (both glass and film side), high visible transmission (>80%), and low film and glass side visible reflection (<15%). Solar transmission above 55% and emissivity below .15 are also required.

The high visible transmission in a metal/dielectric/metal stack is obtained through the constructive interference effects obtained when the optical path lengths of the various layers are correctly matched. Therefore, control over film thickness and oxide stoichiometry are critical to maintaining optimum performance. To be capable of large volume, continuous production, the process must be capable of highly reproduceable deposition conditions to maintain performance parameters within a low standard deviation. Such reproduceability must be maintained over long periods of time, as production equipment goes through periods of shut down, start up, extended maintenance and production of other coatings.

Experimental methods

For purposes of studying the stability of low-emissivity coating production, initial performance parameter control focussed on maintaining visible transmission and emissivity goals, using simple equipment located at the end of the coating line. A transmission monitor was used to maintain visible transmission above 80%. A D&S emissometer[3] was used to maintain emissivity below .15. No other measurements were made of coating properties.